MINISTRY OF EDUCATION AND TRAINING

VIETNAM ACADEMY OF SCIENCE AND TECHNOLOGY

GRADUATE UNIVERSITY OF SCIENCE AND TECHNOLOGY

NGUYEN THI HONG VAN

SYNTHESIS OF PHOTOCATALYTIC COMPOSITE MATERIALS BASED ON UiO-66 AND MIL-101(Cr) UTILIZING WASTE PET FOR ENVIROMENTAL TREATMENT APPLICATIONS

Major: **Theorical and physical chemistry**

Code: **9.44.01.19**

SUMMARY OF DISSERTATION ON THEORICAL AND PHYSICAL CHEMISTRY

Hà Nội – 2025

The dissertation is completed at: Graduate University of Science and Technology, Vietnam Academy Science and Technology

Supervisors:
Supervisors 1: Assoc.Prof.Dr. Pham Xuan Nui
Supervisors 2: Dr. Tran Quang Vinh

Referee 1: ……
Referee 2: …….
Referee 3: …….

The dissertation is examined by Examination Board of Graduate University of Science and Technology, Vietnam Academy of Science and Technology at …….(time, date, month, year)

The dissertation can be found at:
1. Graduate University of Science and Technology Library
2. National Library of Vietnam

INTRODUCTION

1. Rationale of the Dissertation

Metal–organic frameworks (MOFs) are crystalline porous materials featuring extended networks with honeycomb-like cavities. Built from metal ions or clusters and organic linkers whose connectivity and arrangement can be tailored, MOF systems are highly flexible in properties and applications. Chemically recycled terephthalic acid (TPA) from post-consumer PET is a green linker source for synthesizing MOFs that possess substantial specific surface area and notable stability, including UiO-66(Zr) and MIL-101(Cr). However, their intrinsic photocatalytic performance is generally limited and durability can be an issue. Accordingly, a promising research direction is to integrate MOFs with photoactive phases such as TiO_2, carbon quantum dots (CQDs), and various chalcogenides to form MOF composites or hybrids that offer enhanced photocatalytic activity and improved stability. Growing literature has focused on MOF composites that effectively combine the porous architecture, chemical tunability, and structural adjustability of MOFs with the characteristic catalytic, optical, electronic, magnetic, and mechanical merits of photoactive phases; the resulting materials can be rationally engineered to exhibit desirable physicochemical properties alongside high stability and selectivity.

Industrialization—ubiquitous across nations—has delivered modern conveniences but, with its rapid expansion, has also precipitated environmental degradation that threatens ecosystems, human health, and biodiversity. Industrial effluents—dyes from textiles, cosmetics, leather, and food processing, together with antibiotics and plastics—represent hazardous pollutants. While various remediation approaches exist, photocatalysis—an advanced oxidation process (AOP)—has attracted strong interest due to its high efficiency and environmental compatibility.

Motivated by these considerations, this dissertation develops MOF-based composites synthesized using TPA recycled from PET waste and investigates their application to remove recalcitrant organic contaminants in water. The dissertation is entitled:

“Synthesis of Photocatalytic Composite Materials Based on UiO-66 and MIL-101(Cr) Utilizing Recycled PET for Environmental Applications.”

2. Research Objectives

- Recover terephthalic acid (TPA) from PET waste and employ it as the precursor linker to synthesize the MOFs UiO-66 and MIL-101(Cr).

- Fabricate MOF-based nanocomposites with enhanced photoactivity, based on UiO-66 and MIL-101(Cr), for the removal of tetracycline (TC) and polystyrene microplastics (PS MPs) from aqueous environments.

3. Main Research Tasks

- Recycle waste PET bottles to obtain terephthalic acid (TPA) via alkaline hydrolysis for use as a green linker in the synthesis of the MOFs UiO-66(Zr) and MIL-101(Cr).

- Prepare photocatalytic composites using UiO-66 and MIL-101(Cr) as hosts and CQDs, TiO_2, and chalcogenides as active phases.

- Characterize structure, composition, morphology, and properties by XRD, SEM, TEM, FT-IR, N_2 adsorption–desorption (BET), EDX-SEM, UV–Vis, PL, XPS, and DLS.

- Evaluate adsorption–photocatalytic performance toward removal of TC and PS MPs in water.

- Propose preliminary mechanisms for the photocatalytic degradation of TC and PS MPs over the synthesized catalysts.

CHAPTER 1. REVIEW

1.1. Synthesis of MOFs from waste PET

Scaling MOF synthesis for broader industrial use faces challenges related to cost, precursor availability, and synthetic conditions. Recently, sustainable, low-cost strategies have emerged that extract organic and inorganic precursors from recyclable wastes: (i) waste PET bottles as valuable sources of organic linkers; and (ii) electronic and other inorganic solid wastes, including metal-bearing industrial wastewater sludges (e.g., electroplating sludge), refinery wastes, etc., as sources of metal ions.

Global PET consumption exceeds 24 million tons annually (~62.8 billion bottles) and continues to rise. Landfilling or incineration of PET exacerbates environmental problems. Chemical recycling—consistent with the principles of sustainable development—recovers monomers from the original polymer and is considered a viable long-term route. PET hydrolysis has gained increasing interest due to its simplicity and direct integration with PET production. Among routes, alkaline hydrolysis followed by acidification to yield high-purity TPA from PET is particularly effective, providing relatively high yields suitable for MOF synthesis.

Several TPA-linked MOFs have been investigated recently. This dissertation focuses on MIL-101(Cr) and UiO-66 due to their distinctive features. **MIL-101(Cr)** exhibits very high surface area (>4,000 $m^2\ g^{-1}$), together with excellent stability in air, heat, and chemicals, and good moisture resistance—attributes favorable for diverse operating conditions. **UiO-66** is renowned for thermal, chemical, and aqueous stability, arising from strong coordination between Zr(IV) Lewis acid sites and carboxylate oxygens. These features underpin their potential for treating organic pollutants.

Hydro(solvo)thermal synthesis is a classical route to MOFs. In 2009, Cavka et al. reported UiO-66 (University of Oslo-66), constructed from Zr nodes and 1,4-benzene dicarboxylate (BDC). UiO-66 is stable up to ~540 °C and in solvents such as water, acetone, benzene, and DMF. Dyosiba et al. later synthesized UiO-66(Zr) hydrothermally using chemically recycled TPA from waste PET; the material exhibited favorable structure and was effective for hydrogen storage.

Férey et al. synthesized MIL-101(Cr) hydrothermally from $Cr(NO_3)_3 \cdot 9H_2O$, H_2BDC, and HF in Teflon-lined reactors at 493 K for 8 h,

affording blue crystals with surface area and pore volume of ~4,100 $m^2\ g^{-1}$ and 2.0 $cm^3\ g^{-1}$, respectively.

1.2. Composites based on UiO-66 and MIL-101(Cr)

1.2.1. Overview of MOF-based composites

In MOF composites, the merits of MOFs (porosity, chemical tunability, structural adjustability) and the active phases (distinct catalytic, optical, electronic, magnetic properties, and mechanical robustness) can be effectively combined. As a result, new, purpose-designed physicochemical attributes can be realized, enabling superior catalytic performance with enhanced selectivity and stability.

Applications of MOF composites extend beyond canonical MOF uses to adsorption, separations, purification, catalysis, drug delivery, structural tuning, and biomedical fields. The catalytic applications are particularly broad, as different active phases impart distinct functionalities suitable for diverse processes.

Synthetic approaches include encapsulation, impregnation, infiltration, solid grinding, co-precipitation, and more. These methods yield composites where MOFs act either as the continuous phase (matrix) or as the dispersed/reinforcing phase; the former is more common for adsorption, gas storage, and catalysis, often leveraging "bottle-around-ship" (BAS) and "ship-in-a-bottle" (SIB) strategies. Composites have been prepared by solvothermal/hydrothermal, solution precipitation, sonochemical, and microwave methods, among others.

1.2.2. Composites on UiO-66 and MIL-101(Cr)

Representative UiO-66-based composites include: BiOBr/UiO-66 (Sha & Wu) for visible-light degradation of rhodamine B; UiO-66/g-C_3N_4 (Zhang et al.) prepared hydrothermally at 350 °C for 2 h, achieving ~100% methylene blue degradation; and Cu_2O/Fe_3O_4/UiO-66 (Le Thi Thanh Nhi) as a heterogeneous Fenton catalyst removing 84.9% of RB19 in 90 min.

For MIL-101(Cr), Lu Yi et al. synthesized 20%TiO_2@MIL-101(Cr) hydrothermally at 220 °C for 3 h from tetrabutyl titanate and MIL-101(Cr), achieving the highest catalytic activity and up to 70% denitrogenation of fuel within 4 h under visible light.

1.3. Representative photoactive phases in MOF composites

TiO_2 is a widely used photocatalyst but is less active under visible light due to its wide bandgap (E_g ≈ 3.3 eV). Surface modification—metal/non-

metal doping and composite formation—improves visible-light response. For example, TiO_2/g-C_3N_4 (Zhang et al.) exhibits superior activity via Z-scheme heterojunctions that facilitate charge transfer, suppress recombination, and promote radical formation ($\cdot OH$, $\cdot O_2^-$) to degrade RhB. $ZnFe_2O_4$–TiO_2 nanocomposites (Nguyen Thanh Binh et al.) showed excellent visible-light degradation of BPA.

Carbon quantum dots (CQDs) are zero-dimensional nanocarbons (<10 nm). First reported in 2004 (Xu et al.) while purifying SWNTs, CQDs have attracted attention for high water solubility, chemical inertness, low cytotoxicity, strong photoluminescence, and superior catalytic traits. Applications span chemical/biological sensing, bio-labeling, drug delivery, optoelectronics, and metal-free photocatalysis. Synthetic methods include chemical combustion, electrochemical carbonization, microwave irradiation, and hydro/solvothermal treatment of glucose, citric acid, chitosan, banana sap, and proteins.

Chalcogenides contain chalcogen anions (S, Se, Te) and electropositive elements. Ternary chalcogenides of the form X–Y_m–Z_n (X = Cu, Ag, Zn, Cd; Y = Ga, In; Z = S, Se, Te) display outstanding electronic/photophysical properties for photovoltaics, optics, and photocatalysis, and can be synthesized by solvothermal, microwave, or ultrasonic methods. In_2S_3—with a suitable bandgap (2.0–2.5 eV)—is highly attractive for visible-light absorption, exhibiting favorable photoelectric properties and stability. Synthesis routes include CVD, hydrothermal/solvothermal, electrochemical precipitation, microwave-assisted, and chemical bath deposition. Examples include In_2S_3/TiO_2 (Gao et al.) fully degrading methyl orange under visible-UV light, and HPW/TiO_2–In_2S_3 (Heng et al.) with improved imidacloprid degradation due to TiO_2 defects (visible-light response) and type-III band alignment suppressing charge recombination.

1.4. Photocatalytic removal of tetracycline and polystyrene microplastics

Tetracycline (TC), a broad-spectrum antibiotic, contaminates wastewater and poses health risks; conventional treatments are often inadequate. MOFs and MOF composites offer advanced solutions: initially as adsorbents (owing to high surface area/porosity), and increasingly as photocatalysts. For instance, Bi_5O_7I@MIL-101 (Hong et al.) degraded 99% TC in 60 min under visible light via an efficient heterojunction; MIL-

100(Fe)/Bi_2WO_6 (He et al.) achieved 92.4% TC degradation using a direct Z-scheme mechanism.

Microplastics (MPs; <5 mm) are ubiquitous and projected to contribute materially to plastic pollution by 2060. Conventional removal technologies are limited. MOFs can adsorb MPs due to their porosity; e.g., UiO-66-OH@MF-3 on melamine foam (Chen et al.) achieved >95.5% removal with scalability and durability. Photodegradation is another promising route - photocatalysts generate radicals ($\cdot O_2^-$, $\cdot OH$) that oxidize/ mineralize MPs to CO_2 and H_2O. Examples include TiO_2 nanomembranes degrading 98.4% PS under UV; FeB/TiO_2 (Jiehong He) converting PS MPs to H_2; and TiO_2/CuPc (Jingshang) efficiently degrading PS via optimized charge separation.

CHAPTER 2. EXPERIMENTS

2.1. Reagents and materials

Anhydrous NaOH (96%), $HOCH_2CH_2OH$, H_2SO_4 (aq), $ZrOCl_2 \cdot 8H_2O$, $Cr(NO_3)_3 \cdot 9H_2O$ (99%), $AgNO_3$ (99.8%), CuI, $CS(NH_2)_2$ (99%), CH_3CSNH_2 (98%), $C_{12}H_{25}O_4S$, $InCl_3$ (98%), AOM (99%), H_2BDC (99.8%), $Ti[OCH(CH_3)_2]_4$ (TTIP), $(NH_2)_2CO$ (99%), CTAB (≥99%), DMF (99.8%), CH_3COOH, C_4H_8O, HF (40%), HCl (37%), BQ (99%), TBA (99%), $(C_6H_{11}NO_4)$_n, H_2O_2, CH_3OH, C_2H_5OH, NH_4F, $K_2Cr_2O_7$, deionized water, and post-consumer PET bottles.

2.2. Experimental procedures

2.2.1. TPA from waste PET

TPA was obtained by alkaline hydrolysis of PET followed by acidification (scheme omitted here for brevity).

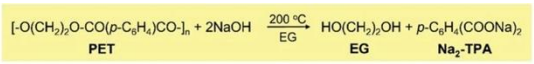

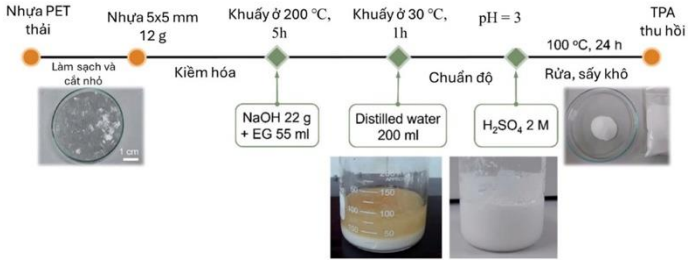

2.2.2. MOFs from recycled TPA

a. MIL-101(Cr): Hydrothermal synthesis from $Cr(NO_3)_3 \cdot 9H_2O$ and TPA in deionized water with a small amount of HF, 220 °C, 9 h. The dark-green crystalline solid was solvent-exchanged with DMF and ethanol, washed with NH_4F solution, and dried to yield green MIL-101(Cr).

b. UiO-66: Solvothermal synthesis from TPA and $ZrOCl_2 \cdot 8H_2O$ in DMF/H_2O/acetic acid at 120 °C for 36 h. The solid was washed with DMF and ethanol and dried to give white UiO-66.

2.2.3. UiO-66-Based Composites

a. CQDs/UiO-66: CQDs were synthesized hydrothermally from chitosan in 1% acetic acid at 180 °C for 12 h. CQDs@UiO-66 was prepared by impregnation: dispersing UiO-66 in ethanol, adding CQD solution, stirring, cooling, and aging, then centrifuging to collect the composite.

b. N-TiO_2/UiO-66: TiO_2 was prepared via sol–gel from TTIP in ethanol and hydrolyzed with water/ethanol/acetic acid with 8 mL, 32 mL và 16 mL, aged 24 h, and dried (100 °C, 12 h). Nitrogen doping used urea (N:Ti = 3:1), followed by drying (100 °C, 12 h) and calcination (450 °C, 3 h, 5 °C min^{-1}) to obtain N-TiO_2. N-TiO_2@UiO-66 was formed solvothermally in ethanol at 120 °C for 24 h, filtered, and dried at 80 °C.

2.2.4. MIL-101(Cr)-based composites

a. CQDs@MIL-101(Cr): Prepared by impregnation, analogous to CQDs@UiO-66.

b. $AgInS_2$@MIL-101(Cr): $AgInS_2$ was first synthesized hydrothermally ($AgNO_3$/$InCl_3$/HCl/TAA, 180 °C, 24 h), washed with ethanol, and dried. Composites with 20–40 wt% $AgInS_2$ were then formed hydrothermally with MIL-101(Cr) at 180 °C for 24 h, washed (hot ethanol, water), and dried; denoted AIS@MIL-101(Cr).

c. $CuInS_2$@MIL-101(Cr): $CuInS_2$ was synthesized solvothermally in ethylene glycol with SDS at 70 °C (pre-mix), then with CuI/$InCl_3$/TAA (molar ratio 1:1:5) at 180 °C for 24 h; washed and dried. CIS@MIL-101(Cr) was then obtained hydrothermally from CIS, $Cr(NO_3)_3 \cdot 9H_2O$, TPA, HF, and water at 180 °C for 12 h; washed (DMF, ethanol) and dried.

d. TiO_2@In_2S_3/MIL-101(Cr): In_2S_3 was synthesized hydrothermally from $InCl_3$ and thiourea in water (150 °C, 6 h). TiO_2, In_2S_3, and $Cr(NO_3)_3 \cdot 9H_2O$ were then dispersed, mixed with TPA and HF, and treated hydrothermally

(180 °C, 12 h). The product, washed (DMF, ethanol) and dried, is denoted TIM.

2.2.5. Evaluation of Pollutant Removal

a. Tetracycline (TC) / Dye RR-195:

For TC (50 ppm, 30 mL), 50 mg catalyst was dispersed and monitored by UV–Vis (λ_max = 357 nm). Removal efficiency:

$$H\% = \frac{(C_o - C)}{C_o} \times 100$$

With the initial solution concentration is denoted as C_0, and the solution concentration at each subsequent time interval is denoted as C.

Radical-quenching experiments identified active species using TBA (·OH), $K_2Cr_2O_7$ (e^-), ammonium oxalate monohydrate (h^+), and BQ ($\cdot O_2^-$) at 10^{-6} M. The trapping experiments were conducted by adding a trapping agent to a TC solution (50 ppm) containing 50 mg of the photocatalyst. Suspensions were stirred in the dark (60 min) before Xe lamp irradiation (300 W); aliquots were withdrawn hourly, filtered, and analyzed.

RR-195 degradation was conducted analogously (λ_max = 541 nm).

b. Polystyrene (PS):

Film degradation: A PS solution in THF was mixed with 0.05 g composite photocatalyst (10 mL), solvent evaporated to form PS–catalyst films. The initial mass (M_1) and the mass after irradiation (M_2) were used to compute:

$$H\% = \frac{(M_1 - M_2)}{M_1} \times 100$$

Suspension degradation: PS suspensions (200 ppm; particle size 0.3–0.4 μm) were treated at room temperature under a 150 W Xe lamp. For 30 mL of PS, 50 mg catalyst was used; suspensions were pre-equilibrated (dark, 90 min). Concentrations were monitored by UV–Vis (λ_max = 290 nm) and removal computed as above.

Simultaneous PS–TC removal: A mixed solution of PS (200 ppm) and TC (30 ppm) at 1:4 (v/v) was equilibrated in the dark (90 min) then irradiated; PS and TC were monitored at 290 nm and 541 nm, respectively.

2.2.6. Characterization

XRD (Bruker D8 Advance, Cu Kα, λ = 1.5406 Å, 2θ = 3–80°);
FT-IR (Shimadzu Affinity-1S, 4000–400 cm^{-1}; KBr pellets/ATR);
Raman (LabRAM HR Evolution, 200–1050 nm);
EDX (JED-2300, JEM-2100F/JED-2300T);

N_2 adsorption–desorption (Micromeritics TriStar 3030, 70 K);
SEM (JEOL JSM-IT200; 2.0 kV BEI, 9.5 nm; 5–300,000×);
TEM (HR-TEM, accelerating voltages 40–200 kV; ≥1,000,000×);
XPS (ESCALab 250, Al Kα, 200–900 μm spot, hemispherical analyzer);
Diffuse reflectance UV–Vis (HO-SP-DRS100, 380–1100 nm);
UV–Vis spectrophotometry (Jasco V-750, 190–900 nm);
PL (Cary Eclipse, Xe flash, 200–900 nm);
HPLC (Shimadzu, UV 255 nm; Heritage MA, 4.6 × 50 mm; 40% ACN/100 mM AmFm, pH 3, 1 mL min^{-1});
DLS (Malvern Zetasizer Nano ZS, 0.3 nm–10 μm, 633 nm, 173°);
EIS (Gamry Reference 600+, 1 mΩ–100 GΩ, ±11 V, 5 MHz max).

CHAPTER 3. RESULTS AND DISCUSSION

3.1. MOFs from PET: Synthesis and Properties

3.1.1. Recovery of TPA

The high purity of terephthalic acid (TPA) recycled from waste PET plastic was evaluated using high-performance liquid chromatography (HPLC). The HPLC chromatogram of the recycled TPA showed a single, dominant peak with a retention time of tR=3.171 min, which is very close to the peak of commercial TPA (tR=3.180 min). The slight difference in retention time is within the acceptable error for HPLC analysis.

Fourier-transform infrared (FT-IR) spectroscopy was also performed on the synthesized TPA and compared to a commercial standard of terephthalic acid. The FT-IR spectrum further confirmed the identity of the product.

These results collectively demonstrate that the chemical recycling of waste PET via alkaline hydrolysis is an effective method for producing high-purity TPA, which can be applied in various industrial sectors.

3.1.2. MIL-101(Cr) and CQDs@MIL-101(Cr): structure and photocatalysis

MIL-101(Cr) synthesized hydrothermally (220 °C, 9 h) showed characteristic XRD peaks at 2θ = 3.29°, 5.11°, 6.02°, 8.48°, 9.05°/10.32° corresponding to (311), (511), (532), (822), and (911) planes. FT-IR bands near 580 cm^{-1} (Cr–O stretching) confirmed coordination between Cr^{3+} and carboxylates; 1500–1700 cm^{-1} bands corresponded to C=O and asymmetric COO^- stretching, with 1512 and 1393 cm^{-1} (C=C) and aromatic ring bands

at 1160, 1017, 885, and 750 cm^{-1}. SEM revealed aggregates of fairly uniform octahedral crystals (300–400 nm). BET analysis indicated a type-I isotherm with surface area (BET) = 1964 $m^2 g^{-1}$ and volume pore = 1.03 $cm^3 g^{-1}$.

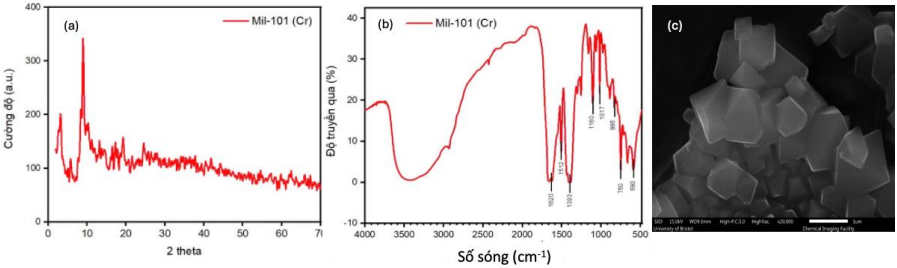

Figure 2: (a) XRD pattern, (b) FT-IR spectrum, and (c) SEM image of MIL-101(Cr)

CQDs@MIL-101(Cr) was prepared by impregnation. XRD/FT-IR retained features of MIL-101(Cr) and CQDs, albeit with reduced intensities due to interactions. SEM showed homogeneous CQD dispersion on MIL-101(Cr). DRS/Tauc indicated visible-light absorption and an apparent bandgap of ~1.98 eV.

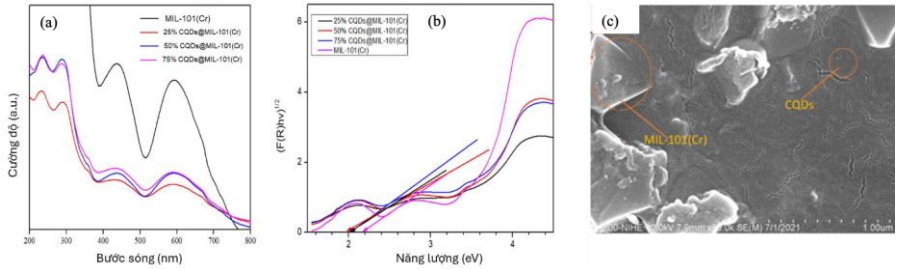

Figure 2: (a) UV-vis-DRS diffuse reflectance spectra and (b) Tauc plot of MIL-101(Cr) and CQDs@MIL-101(Cr), (c) Photograph of CQDs@MIL-101(Cr)

To clarify the separation and recombination of photogenerated electron-hole pairs under light irradiation, the photoluminescence (PL) spectra of the MIL-101(Cr) and CQDs@MIL-101(Cr) materials were measured. The results showed that CQDs@MIL-101(Cr) exhibited the highest inhibition of photogenerated electron-hole recombination, which favors photocatalytic reactions due to its highly efficient charge-carrying components for pollutant treatment.

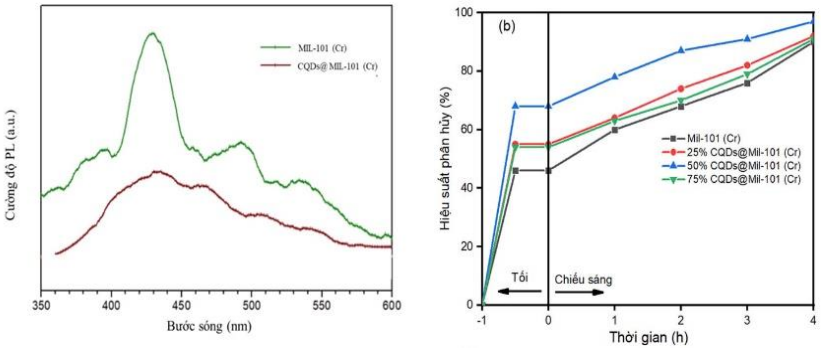

Figure 3: PL spectra of MIL-101(Cr) and CQDs@MIL-101(Cr) and degradation performance.

After evaluating the structural and optical properties of the materials, the 50% CQDs@MIL-101(Cr) catalyst sample demonstrated a high dye degradation efficiency of 96%. This result was achieved under the following conditions: catalyst mass of 50 mg, dye concentration of 50 ppm, reaction time of 4 hours, a 300 W Xenon lamp, and a pH of 6.5.

3.1.3. UiO-66 and CQDs@UiO-66: Structure and Photocatalysis

UiO-66 was obtained hydrothermally at 120 °C for 36 h from recycled TPA. XRD showed main reflections at 2θ = 7.34° and 8.48° ((111), (200)), while FT-IR exhibited bands at 3300, 1653, 1577, 1506, 1398, 814, 746, and 667 cm^{-1}. SEM displayed aggregated particles with primary sizes ~20–30 nm. BET provided surface area (BET) = 1017.27 $m^2 g^{-1}$ and volume pore = 0.55 $cm^3 g^{-1}$.

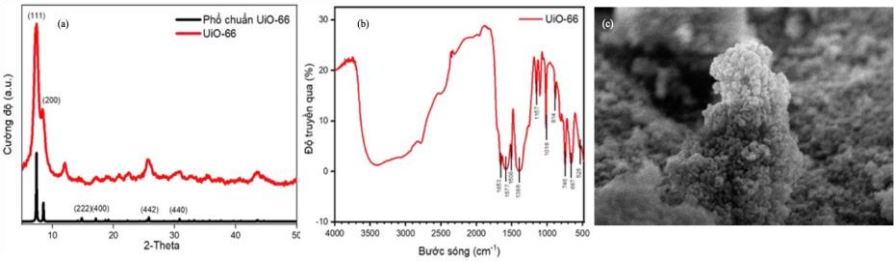

Figure 4: (a) XRD pattern, (b) FT-IR spectrum, and (c) SEM image of UiO-66

The CQDs@UiO-66(Zr) material was synthesized via an impregnation method by dispersing CQDs in a UiO-66/ethanol suspension. The XRD and FT-IR patterns showed the characteristic peaks of both UiO-66 and CQDs present in the CQDs@UiO-66 composite; however, due to mutual

interactions or reduced density of the components during composite formation, along with the dispersion of CQDs on the UiO-66 surface, the peak intensities decreased. Furthermore, diffuse reflectance spectroscopy (DRS) analysis revealed that the CQDs@UiO-66 material is capable of absorbing visible light, with a minimum bandgap energy of 2.4 eV.

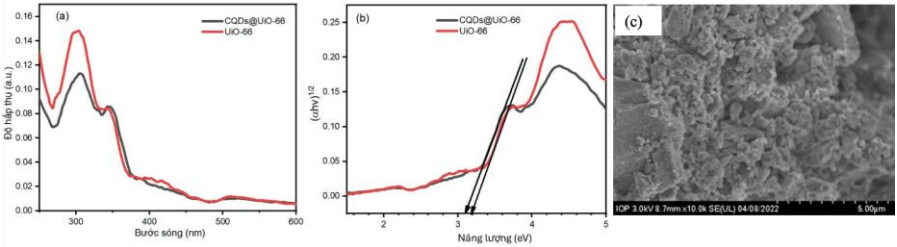

Figure 4: (a) UV-vis-DRS diffuse reflectance spectra and (b) Tauc plot of UiO-66 and CQDs@UiO-66, (c) Photograph of CQDs@UiO-66

The 50% CQDs@UiO-66 sample achieved 99.1% RR-195 degradation; optimal conditions were 50 mg catalyst, 70 ppm dye, 4 h, Xe 300 W.

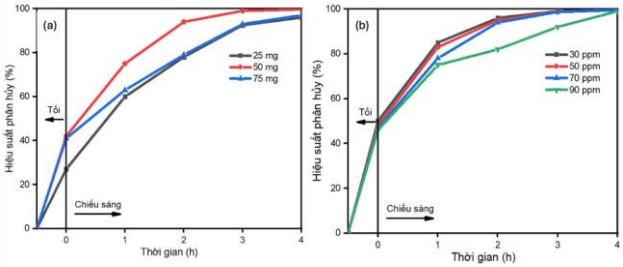

Figure 5: Photocatalytic degradation efficiency of RR-195 using a) varying amounts of CQDs@UiO-66, and b) CQDs@UiO-66 at different RR-195 concentrations (30–90 ppm).

Thus, the 50%CQDs@UiO-66 and 50%CQDs@MIL-101(Cr) composites achieved the highest degradation efficiencies among their respective composite series. However, the maximum degradation efficiency of the MIL-101(Cr) composite (96%) was still lower than that of the UiO-66 composite (99.1%). This can be attributed to the fact that while the MIL-101(Cr) composite has a lower band gap energy (Eg), UiO-66 exhibits superior stability and better interaction with the CQDs, leading to enhanced quantum yield and overall photocatalytic efficiency.

3.2. MIL-101(Cr)-Based Chalcogenide Composites for TC Removal

3.2.1. $AgInS_2$@MIL-101(Cr)

AIS@MIL-101(Cr) was prepared hydrothermally (180 °C, 24 h) from pre-made AIS (180 °C, 24 h) and MIL-101(Cr). XRD, FT-IR, Raman, and XPS confirmed successful composite formation and the presence of Ag^{+}, In^{3+}, Cr^{3+}, and S^{2-}. SEM/TEM showed AIS nanoparticles (~25.3 nm) uniformly distributed on MIL-101(Cr).

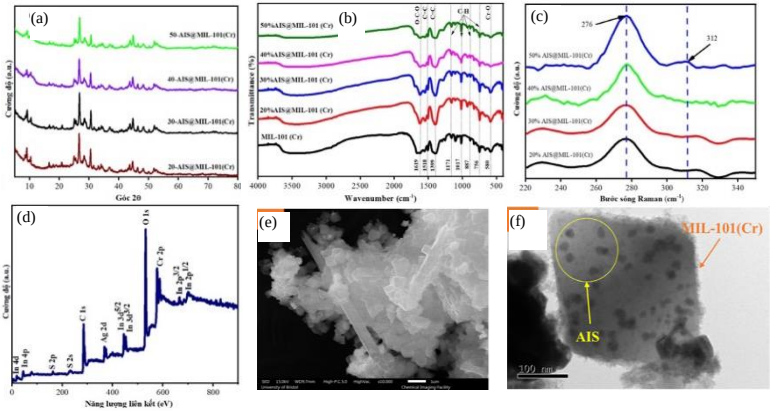

Figure 6: (a) XRD pattern, (b) FT-IR spectrum, (c) Raman spectrum, (d) XPS spectrum, (e) SEM image, and (f) TEM image of the AIS@MIL-101(Cr) material.

EDX indicated Ag, In, S, Cr, O, C at ~0.4, 0.2, 0.7, 0.8, 10.5, and 87.4 at% (approx.). BET revealed microporous character with surface area of BET/volume pore of 1121.03 $m^2.g^{-1}$/0.69 $cm^3.g^{-1}$ for 40% AIS@MIL-101(Cr) and 1964.01 $m^2.g^{-1}$/1.03 $cm^3.g^{-1}$ for pristine MIL-101(Cr), while AIS itself is non-porous.

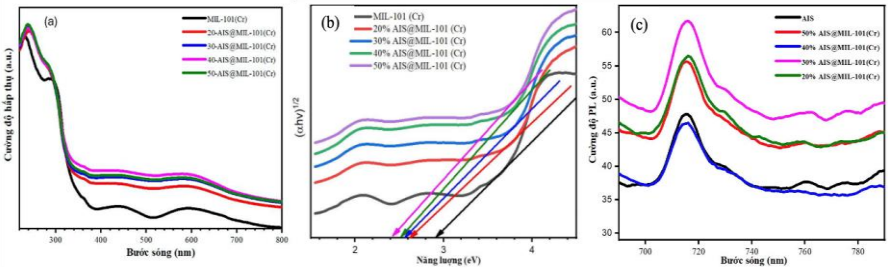

Figure 7: (a) DRS spectra, (b) Tauc plot, and (c) PL spectra of AIS, MIL-101(Cr), and (20-50)% AIS@MIL-101(Cr).

The 40% $AgInS_2$@MIL-101(Cr) composite demonstrates the most effective photocatalytic potential. This is attributed to its strong visible light

absorption, a minimal band gap energy of 2.4 eV, and the highest inhibition of electron-hole recombination. These optical properties align with the experimental results, which showed that this composite achieved the best photocatalytic degradation of tetracycline, reaching approximately 99% degradation after 4 hours of simulated solar light irradiation. This performance significantly surpassed that of pristine AIS, MIL-101(Cr), and other composites with varying AIS content.

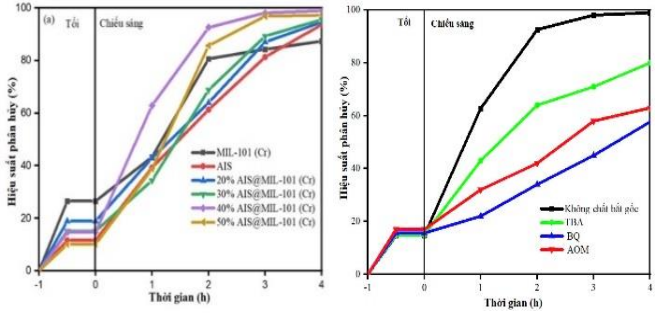

Figure 8: Photocatalytic degradation efficiency with various catalysts (varying AIS content) and TC degradation efficiency of 40% AIS@MIL-101(Cr) with the addition of radical scavengers.

To gain further insight into the mechanism of TC photocatalytic degradation, radical trapping experiments were conducted. The addition of BQ and AOM resulted in a significant decrease in degradation efficiency, indicating that superoxide radicals ($\cdot O_2^-$) and holes (h^+) are the primary active species during the photodegradation process.

Additionally, the reusability of the catalyst was evaluated by performing five consecutive cycles of TC degradation using the 40% AIS@MIL-101(Cr) composite under a 125 W Xenon lamp. The catalyst demonstrated excellent stability, with TC removal efficiencies of 97.4%, 96.3%, 95.7%, and 94.6% for the five successive runs, respectively, compared to the initial run's efficiency of 98.9%.

3.2.2. $CuInS_2$@MIL-101(Cr)

CIS@MIL-101(Cr) was synthesized via a one-pot hydrothermal route from pre-formed CIS and in-situ MIL-101(Cr) (with recycled TPA) at 180 °C for 12 h. Structural (XRD, FT-IR, Raman, XPS) and morphological (SEM/TEM) characterizations confirmed successful composite formation.

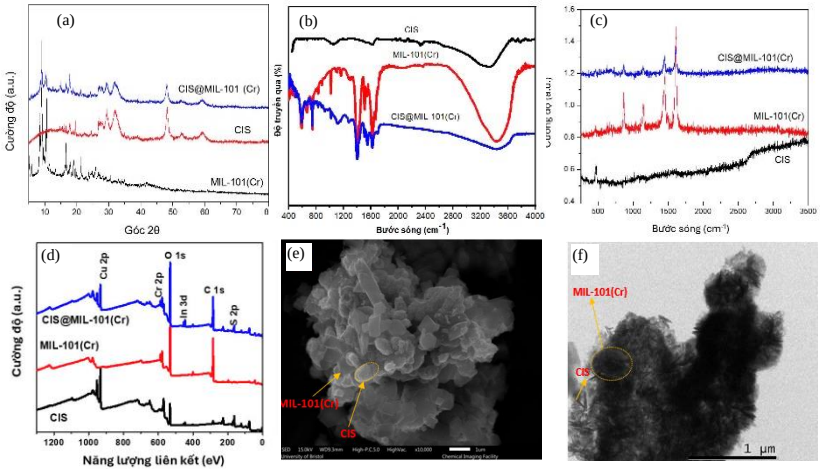

Figure 9: (a) XRD pattern, (b) FT-IR spectrum, (c) Raman spectrum, (d) XPS spectrum, (e) SEM image, and (f) TEM image of the CIS@MIL-101(Cr) material.

The 40% CIS@MIL-101(Cr) sample exhibited low apparent bandgaps (~1.26 and 1.95 eV) and achieved 98.2% TC degradation under visible light in 5 h, slightly below 40% AIS@MIL-101(Cr). Kinetics followed pseudo-first-order behavior. Radical trapping indicated that h^+, e^-, and especially $\cdot O_2^-$ were dominant in CIS-based degradation; for AIS composites, h^+ and $\cdot O_2^-$ were also key.

Thus, although the two chalcogenides, $AgInS_2$ and $CuInS_2$, have different optical properties, their similar electronic components and structural characteristics lead to comparable photocatalytic performance and degradation mechanisms for TC when composited with the same MIL-101(Cr) support.

3.3. MOF-Based Composites for PS Microplastic Removal

PS suspensions (200 ppm) in THF/H_2O (1:4 v/v) had DLS-measured particle sizes of 0.3–0.4 µm.

3.3.1. N-TiO_2@UiO-66

XRD evidenced both N-TiO_2 and UiO-66 phases in the composite; SEM showed ~15–20 nm N-TiO_2 particles dispersed on aggregated UiO-66. DRS/Tauc indicated $E_g \approx 2.3$ eV for N-TiO_2@UiO-66 (vs. 2.9 eV for UiO-66), demonstrating improved visible-light absorption.

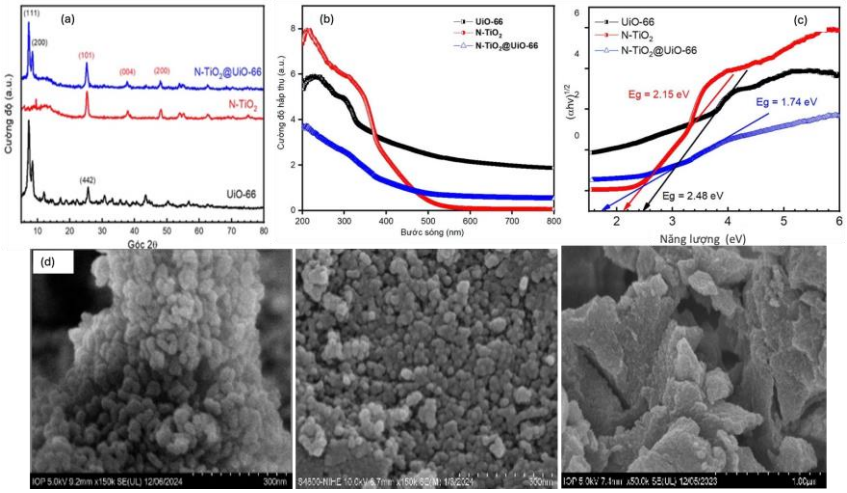

Figure 10: (a) XRD pattern, (b) DRS spectrum, (c) Tauc plot, and (d) SEM image of UiO-66, N-TiO_2, and N-TiO_2@UiO-66.

PS film degradation: mass loss reached 25% after 4 weeks and 36% after 9 weeks (150 W Xe lamp).

PS suspension: nearly 100% PS removal after 24 h irradiation (150 W Xe lamp).

3.3.2. TiO_2@In_2S_3/MIL-101(Cr) (TIM)

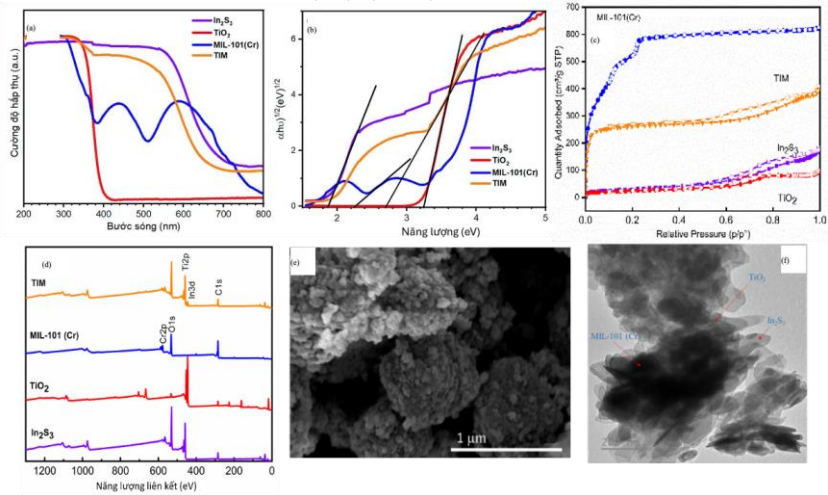

Figure 11: (a) DRS spectrum, (b) Tauc plot, (c) N_2 adsorption-desorption isotherm, (d) XPS spectrum, (e) SEM image, and (f) TEM image of TiO_2@In_2S_3/MIL-101(Cr).

TIM was synthesized hydrothermally (TiO_2, In_2S_3, Cr precursor, and recycled TPA). The nanocomposite showed high adsorption capacity (surface area of BET ≈ 956 $m^2.g^{-1}$; volume ≈ 0.604 $cm^3.g^{-1}$) and strong visible-light response ($E_g \approx 2.7$ eV).

For TC alone (30 $mg.L^{-1}$), TIM (0.3 $g.L^{-1}$) removed 98.67% within 180 min at pH=5 (300 W Xe lamp).

For PS:

- *Film*: PS–TIM films exhibited rapid mass loss over 6 weeks (41.6%), reaching 46.6% after 9 weeks - exceeding N-TiO_2@UiO-66 films.

- *Suspension*: PS adsorption rose from 53.73% to 97.93% within 15-75 min.

Notably, when treating a mixture of PS MPs (200 ppm) and TC (30 ppm) in a solvent mixture, the TIM nanocomposite achieved 78% PS adsorption after 90 minutes, with complete removal after 180 minutes of irradiation. The slower removal rate of PS in the mixture compared to a single-component system is attributed to the competitive adsorption of TC on the catalyst surface, which hinders PS access to the active sites. The removal efficiency for TC reached 99.9% after 4 hours of irradiation.

Furthermore, the TIM nanocomposite demonstrated high stability and reusability, maintaining a TC degradation efficiency of 95% and a PS adsorption efficiency of 94% after five cycles. This exceptional performance is a result of the strong interface between the active phases and the efficient electron transfer mechanism between TiO_2 and In_2S_3.

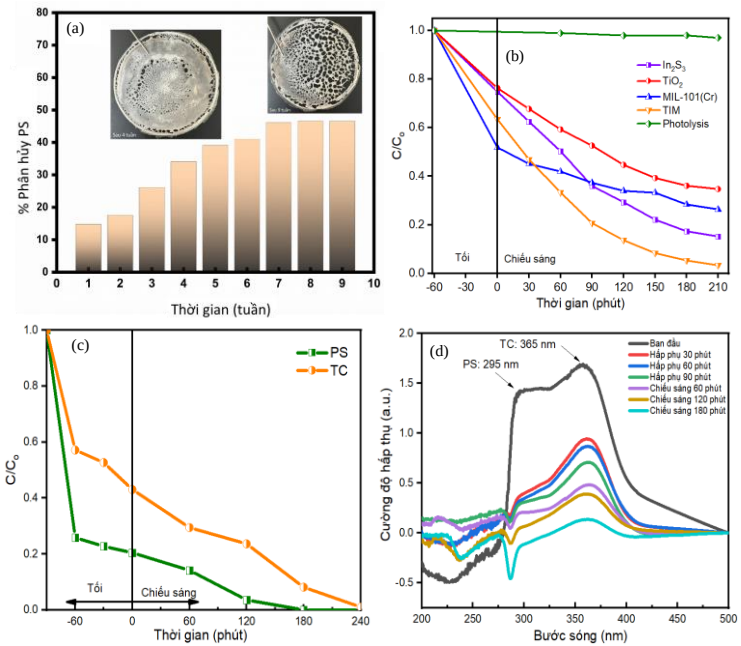

Figure 12: (a) PS degradation efficiency of the PS-(TiO_2@In_2S_3/MIL-101(Cr)) thin film under visible light, (b) C/Coversus reaction time for In_2S_3, TiO_2, MIL–101(Cr) and TIM nanocomposite, (c) Removal efficiency and (d) UV–Vis spectra illustrating the simultaneous removal of PS (200 ppm) and TC (30 ppm) in water by the TIM nanocomposite.

CONCLUSIONS AND RECOMMENDATIONS

Conclusions

- UiO-66 and MIL-101(Cr) were successfully synthesized from recycled TPA (from PET), with specific surface areas of 1017.27 and 1964.01 $m^2.g^{-1}$, respectively. XRD/FT-IR/SEM matched literature data for materials made from commercial TPA. CQDs@UiO-66 and CQDs@MIL-101(Cr) exhibited excellent RR-195 degradation, with optimal CQD loading at 50 wt%. Although MIL-101(Cr) composites showed stronger dark adsorption (due to higher surface area), UiO-66 composites achieved higher photocatalytic removal (99.1% vs. 96%), likely due to UiO-66's superior stability and interfacial synergy with CQDs.

- Additional composites $AgInS_2$@MIL-101(Cr), $CuInS_2$@MIL-101(Cr), N-TiO_2@UiO-66, and TiO_2@In_2S_3/MIL-101(Cr)—were prepared to treat recalcitrant organics.

+ Chalcogenide group (I–III–VI_2): 40% $AgInS_2$@MIL-101(Cr) ($E_g \approx$ 2.4 eV) and 40% $CuInS_2$@MIL-101(Cr) ($E_g \approx$ 1.26/1.95 eV) exhibited strong visible-light activity and suppressed recombination (PL), degrading TC by ~99% (AIS) in 4 h and 98.2% (CIS) in 5 h. Kinetics were pseudo-first-order; $\cdot O_2^-$ and h^+ were dominant reactive species (AIS), while h^+, e^-, and especially $\cdot O_2^-$ dominated for CIS.

+ TiO_2-based group: N-TiO_2@UiO-66 and TIM effectively removed PS MPs (film and suspension), and TIM enabled simultaneous PS–TC removal (PS: 78% after 90 min adsorption, 100% after 180 min irradiation; TC: 99.9% after 4 h), with excellent recyclability.

Recommendations

- Expand the library of UiO-66(Zr)-based photocatalysts to strengthen comparative insights versus MIL-101(Cr), guiding practical selection of TPA-linked MOF composites (leveraging recycled PET) for real-world treatment of recalcitrant organic wastes.

- Broaden research on photocatalysts for microplastic remediation, with deeper mechanistic studies on adsorption and photo-oxidation of PS and other MPs across the synthesized materials.

NOVEL CONTRIBUTIONS OF THE DISSERTATION

- Established a process to obtain TPA from PET waste and synthesized UiO-66 and MIL-101(Cr) from recycled TPA; evaluated CQD-based composites of both MOFs for RR-195 degradation.

- Developed new MOF-based photocatalysts combining UiO-66/MIL-101(Cr) with photoactive phases (TiO_2, chalcogenides):

- First application of I–III–VI_2 ($AgInS_2$, $CuInS_2$) chalcogenide composites on MIL-101(Cr) for TC degradation, including preliminary mechanistic insights.

- First assessment of PS microplastic removal using UiO-66- and MIL-101(Cr)-based composites, including simultaneous PS–TC remediation in water.

LIST OF THE PUBLICATIONS RELATED TO THE DISSERTATION

1. Xuan N. Pham, Van-Tai Vu, Hong Van T. Nguyen, T.-Thanh-Bao Nguyen, Huan V. Doan, "Designing a novel heterostructure $AgInS_2$@MIL-101(Cr) photocatalyst from PET plastic waste for tetracycline degradation," *Nanoscale Advances* (2022).
2. Hong Van T. Nguyen, Manh B. Nguyen, Huan V. Doan, Xuan Nui Pham, "A green synthesis of $CuInS_2$/MIL-101(Cr) nanocomposite with efficient visible-light-induced photocatalytic activity," *Materials Research Express* **10** (2023) 085506.
3. Nguyen Thi Hong Van, Nguyen Thi Tra, Pham Xuan Nui, "Synthesis of CQDs/MIL-101(Cr) photocatalytic nanocomposite for degradation of RR-195," *Vietnam Journal of Catalysis and Adsorption* **13**(1) (2024) 106–112.
4. Nguyen Thi Phuong Lan, Nguyen Thi Hong Van, Duong Thi Thuy Trang, Xuan Nui Pham, "High efficiency of CQDs/UiO-66 photocatalytic nanocomposite for degradation of RR-195 under visible irradiation," *Vietnam Journal of Catalysis and Adsorption* **13**(3) (2024) 1–7.